

# Biaxial Strain based Performance Modulation of Negative-Capacitance FETs

Moonhoi Kim, Junbeom Seo, and Mincheol Shin<sup>†</sup>  
 School of Electrical Engineering  
 Korea Advanced Institute of Science and Technology  
 Daejeon, Republic of Korea  
<sup>†</sup>e-mail: [mshin@kaist.ac.kr](mailto:mshin@kaist.ac.kr)

**Abstract**—In this work, we report device simulations conducted to study the performance of biaxially strained ferroelectric-based negative capacitance FETs (NCFETs). We adopted  $\text{PbZr}_{0.5}\text{Ti}_{0.5}\text{O}_3$  (PZT) and  $\text{HfO}_2$  as ferroelectric materials and applied biaxial strain using the first-principles method. It was found that PZT and  $\text{HfO}_2$  show different trends in the negative capacitance (NC) region under biaxial strain. Biaxial strain strongly affects the NC of PZT, whereas  $\text{HfO}_2$  is not as susceptible to biaxial strain as PZT. When no strain is applied,  $\text{HfO}_2$ -based NCFETs exhibit a better performance than PZT-based NCFETs. However, the subthreshold slope and ON-state current are improved in the case of PZT-based NCFETs when the compressive biaxial strain is increased, whereas the performance of  $\text{HfO}_2$ -based NCFETs is slightly degraded. In particular, the negative drain-induced barrier lowering and negative differential resistance vary considerably when compressive strain is applied to PZT-based NCFETs.

**Keywords**—PZT,  $\text{HfO}_2$ , strain, negative capacitance FETs, ferroelectrics, density functional theory

## I. INTRODUCTION

As conventional MOSFETs continue to be downscaled at a fast pace, inefficient power dissipation has become the most prominent issue in nanoelectronics [1]. This has resulted in extensive studies on steep-slope devices that can overcome the “Boltzmann tyranny,” such as tunneling FETs [2], [3] and negative capacitance FETs (NCFETs) [4], [5]. In particular, mainly because of their high performance and novel operation mechanism, NCFETs have recently drawn a lot of attention. It has been reported that a ferroelectric (FE) material integrated into the gate stack of conventional MOSFETs has a negative capacitance (NC) that can boost the device performance by improving both the subthreshold swing (SS) and ON-state current ( $I_{\text{ON}}$ ) [6]. In addition, interesting results have been found on negative drain-induced barrier lowering (DIBL) and negative differential resistance (NDR), which are not exhibited in conventional MOSFETs [7], [8].

To enhance the performance of NCFETs, the ferroelectricity of the FE layer needs to be improved. To do so, strain engineering has been used to modulate the ferroelectricity through lattice mismatch [9]. Recent studies have shown that inducing a high compressive strain of above 2% on perovskite

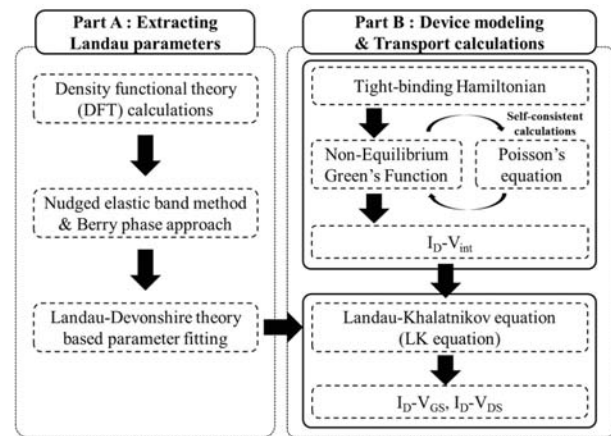


Fig. 1. Flowchart of the NCFET simulation.

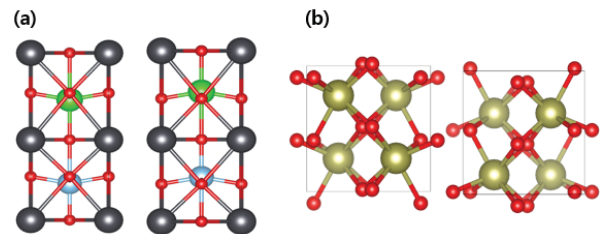


Fig. 2. Two stable states of (a) PZT and (b)  $\text{HfO}_2$  used in the DFT calculations. The large black, green, blue, and gold spheres indicate Pb, Zr, Ti, and Hf, respectively, and the small red spheres represent O.

FE materials is possible [10], [11]. Moreover, after FE properties were discovered in  $\text{HfO}_2$ , significant attention has been paid to the strain effects on  $\text{HfO}_2$  [12], [13]. However, the effects of strain on the transport characteristics of NCFETs, which are expected to affect the device performance, have yet to be studied. In this work, we conducted a computational study on the performance of biaxially strained FE-based NCFETs. PZT and  $\text{HfO}_2$  were adopted as the FE materials, and biaxial strain was applied by using the first-principles method. We conducted quantum-mechanical device simulations and compared the performance of PZT- and  $\text{HfO}_2$ -based NCFETs.

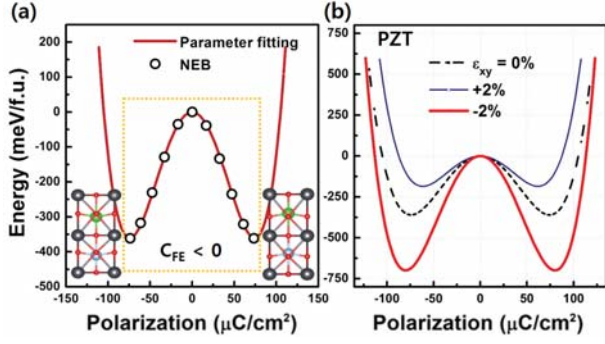


Fig. 3. Free energy as a function of the polarization in perovskite PZT, calculated using two stable PZT structures. (a) The NEB trajectories (circles) have been fitted with  $U = \alpha P^2 + \beta P^4 + \gamma P^6$  (red line). Nine images of the NEB method were used in the calculations. (b) The variation in FE properties with biaxial strain.

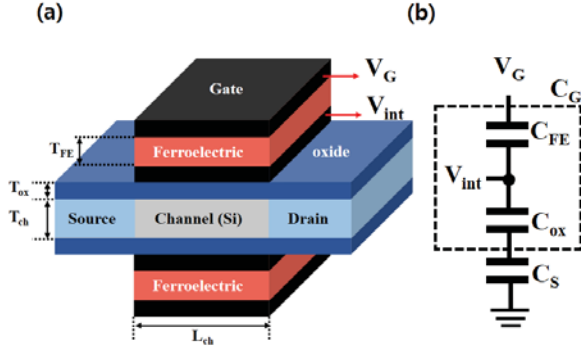


Fig. 4. (a) Schematic diagram of UTB double-gate NCFETs and (b) equivalent circuit model consisting of ferroelectric ( $C_{FE}$ ), dielectric ( $C_{ox}$ ), and semiconductor capacitors ( $C_s$ ).  $C_G$  is the series capacitance of  $C_{FE}$  and  $C_{ox}$ . The channel length ( $L_{ch}$ ), channel thickness ( $T_{ch}$ ), and equivalent oxide thickness ( $T_{ox}$ ) are 20, 3, and 1.5 nm, respectively. The source and drain region are n-doped with  $5 \times 10^{20} \text{ cm}^{-3}$ , and the drain voltage ( $V_D$ ) is 0.5 V.

## II. SIMULATION DETAILS

The overall simulation procedure, shown in Fig. 1, consists of two parts: extracting the Landau parameters (Part A), and conducting device modeling and transport calculations (Part B). The biaxial strain was imposed on the FE materials using density functional theory (DFT) calculations. The Landau parameters were extracted from the DFT results. NCFET device modeling and transport calculations were then conducted.

### A. Extracting Landau Parameters

For a geometry optimization of the FE materials, first-principles DFT calculations were employed using the OpenMX package with the local density approximation exchange correlation functional [14]. We chose a linear combination of atomic orbitals basis set with a  $2s^1 2p^3 2d^6 1f^7$ . In all of the calculations, the atomic structures were fully relaxed until the residual forces were less than  $0.01 \text{ eV/\AA}$ . The fully relaxed

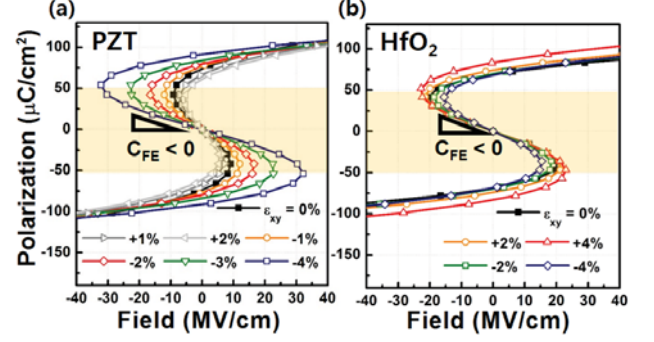


Fig. 5. Polarization ( $P$ ) as a function of electric field of biaxially strained (a) PZT and (b)  $\text{HfO}_2$ . “+” denotes the tensile strain and “-” denotes the compressive strain.

atomic structures are shown in Fig. 2. For the PZT-based NCFETs, we considered a supercell  $1 \times 1 \times 2$  tetragonal PZT, as shown in Fig. 2(a) [15]. The calculated strain-free lattice constants were  $a_1 = a_2 = 3.97 \text{ \AA}$  and  $a_3 = 8.29 \text{ \AA}$ , which are comparable to the experimental and the simulation results [16]. For the  $\text{HfO}_2$ -based NCFETs,  $\text{HfO}_2$  shown in Fig. 2(b) yielded similar strain-free lattice constants as in the previous simulation results [17], [18]. The strain was then biaxially imposed on the unstrained structure within the range  $\pm 4\%$ .

Potential barriers of the polarization switching pathways, which are important properties of FE materials, were determined using the nudged elastic band method (NEB). The polarizations for the bulk systems were calculated using the Berry phase approach. The Landau free energy ( $U$ ) of the FE material is defined using the Landau–Devonshire theory [19] as

$$U = \alpha P^2 + \beta P^4 + \gamma P^6 - E \cdot P \quad (1)$$

where the Landau parameters,  $\alpha$ ,  $\beta$ , and  $\gamma$ , which vary with the biaxial strain, were extracted from the DFT results. Fig. 3(a) shows the results of the fitted free energy of PZT where the external field ( $E$ ) is absent, and the region of NC is highlighted with the dotted square. In the case of unstrained PZT, the fitted Landau parameters— $\alpha = -2.25 \times 10^8 \text{ m/F}$ ,  $\beta = 2.87 \times 10^8 \text{ m}^5/\text{F/C}^2$ , and  $\gamma = 1.00 \times 10^8 \text{ m}^9/\text{F/C}^4$ —are in good agreement with the results of the previous work [20]. Biaxial strain was applied to fully relaxed structures of PZT, and the Landau parameters were extracted, as shown in Fig. 3(b).

### B. Device Modeling and Transport Calculations

We simulated ultra-thin body (UTB) double-gate NCFETs, as shown in Fig. 4(a). The baseline MOSFETs and FE capacitor were modeled separately [8]. Non-equilibrium Green’s function equation was self-consistently solved with a Poisson equation in the ballistic transport regime using our in-house tool for the baseline MOSFETs, whose channel region was modeled using tight-binding Hamiltonians.

The FE layer, which amplifies the gate voltage of the baseline MOSFET, was modeled based on the Landau–Khalatnikov (LK) equation. The LK equation [21] is defined as

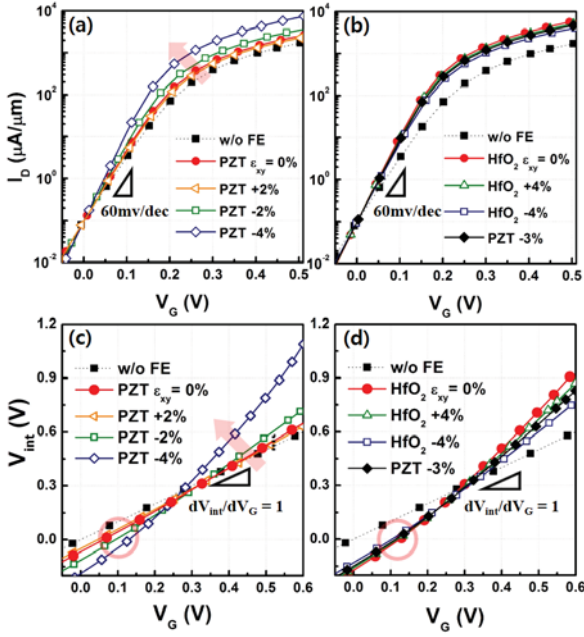


Fig. 6.  $I_D$  versus  $V_G$  of NCFETs for various  $\epsilon_{xy}$  when the thickness of the FE layer ( $T_{FE}$ ) is 40 nm in the case of (a) PZT- and (b) HfO<sub>2</sub>-based NCFETs.  $V_{int}$  versus  $V_G$  for various  $\epsilon_{xy}$ , in the case of (c) PZT- and (d) HfO<sub>2</sub>-based NCFETs.

$$\rho \frac{dP}{dt} + \nabla_p U = 0 \quad (2)$$

where  $\rho$  and  $P$  are the resistivity and polarization, respectively. When the FE is under a steady state ( $dP/dt = 0$ ),  $E$  can be written as

$$E = 2\alpha P + 4\beta P^3 + 6\gamma P^5 \quad (3)$$

which is induced through the polarization of the FE layer. Fig. 4(b) shows an equivalent capacitance model of the simulated NCFETs, where the internal voltage ( $V_{int}$ ) is the voltage amplified by the FE layer when the gate voltage ( $V_G$ ) is applied.

### III. SIMULATION RESULTS

#### A. DFT Results of PZT and HfO<sub>2</sub>

Figs. 5(a) and (b) illustrate the polarization characteristics of PZT and HfO<sub>2</sub>, respectively. In the case of PZT, the slope in the highlighted NC region is significantly changed by biaxial strain. The slope decreases when compressive strain is applied, whereas the tensile strain tends to provide an opposite effect. Consequently, the biaxial strain strongly affects the NC properties of PZT. In contrast, for the case of HfO<sub>2</sub>, the slope does not change as much, which indicates that the NC of HfO<sub>2</sub> is not as susceptible to biaxial strain as PZT.

#### B. Transfer Characteristics of NCFETs

Figs. 6(a) and (b) show the hysteresis-free transfer curves of PZT- and HfO<sub>2</sub>-based NCFETs, respectively. The curves are shifted to have an OFF-state current of 0.1  $\mu\text{A}/\mu\text{m}$  at  $V_G = 0.0$

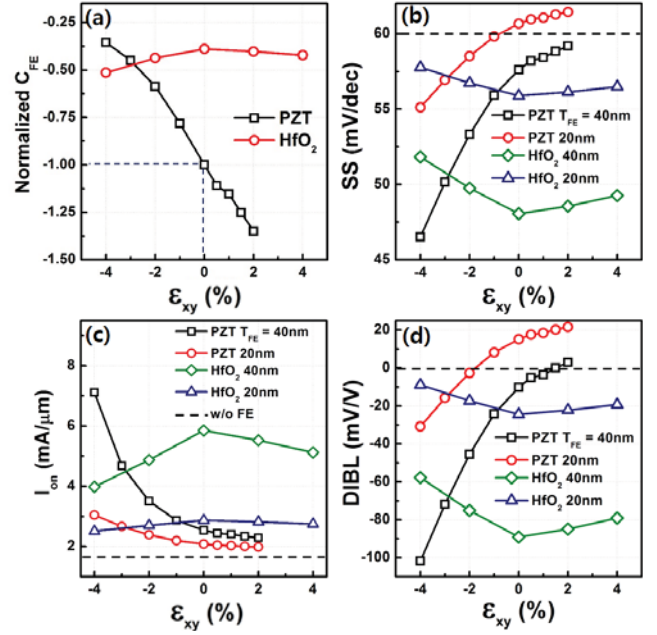


Fig. 7. (a) Normalized  $C_{FE}$  versus  $\epsilon_{xy}$ .  $C_{FE}$  is normalized by the capacitance of PZT of  $\epsilon_{xy} = 0\%$ . (b) SS, (c)  $I_{ON}$ , and (d) DIBL as functions of  $\epsilon_{xy}$ .

$V$ . As shown in the figures, PZT-based NCFETs show a strong variation in strain, whereas HfO<sub>2</sub>-based NCFETs do not. One of the important factors in determining the transfer characteristics is the degree of voltage amplification in the FE layer. If  $dV_{int}/dV_G$  is larger than 1, NCFETs achieve a better performance than conventional baseline MOSFETs. The amplification of  $V_{int}$  at a certain  $V_G$  for various rates of biaxial strain ( $\epsilon_{xy}$ ) is shown in Figs. 6(c) and (d). In the case of  $\epsilon_{xy} = 0\%$  (red circle), HfO<sub>2</sub>-based NCFETs show a steeper  $dV_{int}/dV_G$  than PZT-based NCFETs. However, as shown in Fig. 6(c),  $dV_{int}/dV_G$  becomes steeper as the compressive biaxial strain increases in the case of PZT-based NCFETs. With HfO<sub>2</sub>-based NCFETs, on the other hand,  $dV_{int}/dV_G$  is insensitive to strain, and has a similar value to that of PZT with a compressive strain of 3% (black rhombus), as shown in Fig. 6(d). With a compressive strain of over 4%, PZT-based NCFETs can therefore provide a better performance than HfO<sub>2</sub>-based NCFETs.

#### C. Device Performance of NCFETs

The variation in  $C_{FE}$  with  $\epsilon_{xy}$  is plotted in Fig. 7(a). In the case of PZT, normalized  $C_{FE}$  monotonically increases with the increase in compressive strain. However, HfO<sub>2</sub> is relatively insensitive to biaxial strain, and normalized  $C_{FE}$  has the largest value when  $\epsilon_{xy}$  is 0%. This tendency of  $C_{FE}$  is related to the SS,  $I_{ON}$ , and DIBL, as shown in Fig. 7.

To enhance SS and  $I_{ON}$ , the compressive strain is effective for PZT-based NCFETs, whereas an unstrained FE layer is preferred for HfO<sub>2</sub>-based NCFETs. The dependence of SS and  $I_{ON}$  on  $\epsilon_{xy}$  is shown in Figs. 7(b) and (c), respectively. The SS, which is inversely proportional to  $C_G = (1/C_{ox} + 1/C_{FE})^{-1}$ , shows

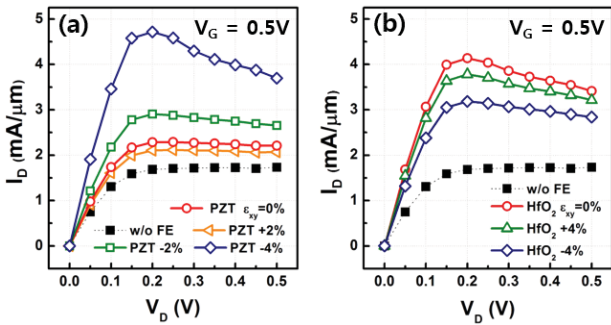


Fig. 8. NDR for (a) PZT- and (b) HfO<sub>2</sub>-based NCFETs, where  $V_G$  and  $T_{FE}$  are 0.5 V and 30 nm, respectively.

a similar tendency with normalized  $C_{FE}$ , as indicated in Fig. 7(b). In the case of PZT-based NCFETs, SS is significantly improved as  $\epsilon_{xy}$  decreases, whereas HfO<sub>2</sub>-based NCFETs are relatively insensitive to  $\epsilon_{xy}$  and have the greatest SS when  $\epsilon_{xy}$  is 0%. Similarly, as shown in Fig. 7(c), the compressive strain enhances  $I_{ON}$  of PZT-based NCFETs, whereas it slightly degrades  $I_{ON}$  of HfO<sub>2</sub>-based NCFETs. The strain effects increase when  $T_{FE}$  increases. When strain is applied to PZT-based NCFETs of 40 nm thickness, greater improvement in SS and  $I_{ON}$  occurs compared to the case of 20 nm thickness. The tensile strain degrades  $I_{ON}$  of both PZT- and HfO<sub>2</sub>-based NCFETs.

DIBL can be modulated through the application of biaxial strain, as shown in Fig. 7(d). HfO<sub>2</sub>-based NCFETs show a relatively strain-insensitive and large negative DIBL. On the other hand, in the case of PZT-based NCFETs, the negative DIBL gradually increases with the compressive strain. It should be noted that a proper biaxial strain can lead to a DIBL of 0 mV/V at a certain  $T_{FE}$ : in the case of  $T_{FE} = 20$  nm PZT, a compressive biaxial strain of 2% provides a DIBL of 0 mV/V.

PZT-based NCFETs under strong compressive strain exhibit a large NDR, as shown in Figs. 8(a) and (b). When no strain is applied (red circle), PZT-based NCFETs show a relatively small NDR compared to HfO<sub>2</sub>-based NCFETs. If a compressive strain of 4% is applied, the NDR effect becomes larger in PZT-based NCFETs than in HfO<sub>2</sub>-based NCFETs.

#### IV. CONCLUSION

A detailed study on the biaxial strain effects on NCFETs has been performed by means of extraction of FE parameters based on the DFT method. We have found that PZT exhibits a large variation in NC with biaxial strain, whereas a much smaller change was observed for HfO<sub>2</sub>. We conclude that the application of compressive strain can boost the performance of PZT-based NCFETs, whereas an unstrained FE layer is preferred for HfO<sub>2</sub>-based NCFETs. Moreover, an appropriate biaxial strain can provide a DIBL of 0 mV/V at a certain  $T_{FE}$  and large NDR.

#### Acknowledgment

This work was supported by Samsung Research Funding & Incubation Center of Samsung Electronics under Project Number SRFC-TA1703-10.

#### REFERENCES

- [1] S. Takagi, T. Irisawa, T. Tezuka, T. Numata, S. Nakaharai, N. Hirashita, Y. Moriyama, K. Usuda, E. Toyoda, S. Dissanayake, M. Shichijo, R. Nakane, S. Sugahara, M. Takenaka, and N. Sugiyama, "Carrier-transport-enhanced channel CMOS for improved power consumption and performance," *IEEE Trans. Electron Dev.*, vol. 55, no. 1, pp. 21–39, Jan. 2008.
- [2] W. Choi, B. G. Park, J. D. Lee, and T. J. K. Liu, "Tunneling field-effect transistors (TFETs) with subthreshold swing (SS) less than 60 mV/dec," *IEEE Electron Device Lett.*, vol. 28, no. 8, pp. 743–745, 2007.
- [3] A. M. Ionescu and H. Riel, "Tunnel field-effect transistors as energy-efficient electronic switches," *Nature*, vol. 479, no. 7373, pp. 329–337, Nov. 2011.
- [4] S. Salahuddin and S. Datta, "Use of negative capacitance to provide voltage amplification for low power nanoscale devices," *Nano Lett.*, vol. 8, no. 2, pp. 405–410, 2007.
- [5] A. Rusu, G. A. Salvatore, D. Jimenez, and A. M. Ionescu, "Metalferroelectric-meta-oxide-semiconductor field effect transistor with sub-60 mV/decade subthreshold swing and internal voltage amplification," in *Proc. IEEE Int. Electron Devices Meeting (IEDM)*, pp. 16.3.1–16.3.4., Dec. 2010.
- [6] A. I. Khan, K. Chatterjee, B. Wang, S. Drapcho, L. You, C. Serrao, S. R. Bakaul, R. Ramesh, and S. Salahuddin, "Negative capacitance in a ferroelectric capacitor," *Nature Mater.*, vol. 14, no. 2, pp. 182–186, 2015.
- [7] J. Zhou, G. Han, Y. Liu, Y. Peng, J. Zhang, Q. Sun, D. W. Zhang, and Y. Hao, "Negative Differential Resistance in Negative Capacitance FETs," *IEEE Electron Device Letters*, vol. 39, no. 4, pp. 622–625, 2018.
- [8] J. Seo, J. Lee, and M. Shin, "Analysis of drain-induced barrier rising in short-channel negative-capacitance FETs and its applications," *IEEE Trans. Electron Devices*, vol. 64, no. 4, pp. 1793–1798, Apr. 2017.
- [9] D. G. Schlom, L.-Q. Chen, C.-B. Eom, K. M. Rabe, S. K. Streiffer, and J.-M. Triscone, "Strain tuning of ferroelectric thin films," *Annu. Rev. Mater. Res.*, vol. 37, no. 1, pp. 589–626, May 2007.
- [10] I. Fina, N. Dix, J. M. Rebled, P. Gemeiner, X. Marti, F. Peiro, B. Dkhil, F. Sanchez, L. Fabrega, and J. Fontcuberta, "The direct magnetoelectric effect in ferroelectric–ferromagnetic epitaxial heterostructures," *Nanoscale*, vol. 5, no. 17, pp. 8037–8044, 2013.
- [11] J. Lyu, I. Fina, R. Solanas, J. Fontcuberta, and F. Sanchez, "Tailoring Lattice Strain and Ferroelectric Polarization of Epitaxial BaTiO<sub>3</sub> Thin Films on Si (001)," *Scientific reports*, vol. 8, no. 495, 2018.
- [12] P. Polakowski and J. Müller, "Ferroelectric in undoped hafnium oxide," *Appl. Phys. Lett.*, vol. 106, no. 23, pp. 232905-1–232905-5, Jun. 2015.
- [13] S. Clima, D. J. Wouters, C. Adelman, T. Schenk, U. Schröder, M. Jurczak, and G. Pourtois, "Identification of the ferroelectric switching process and dopant-dependent switching properties in orthorhombic HfO<sub>2</sub>: A first principles insight," *Appl. Phys. Lett.*, vol. 104, no. 9, p. 092906, 2014.
- [14] T. Osaki and H. Kino, "Efficient projector expansion for the ab initio LCAO method," *Phys. Rev. B, Condens. Matter*, vol. 72, pp. 045121-1–045121-8, Jul. 2003.
- [15] Z. Wu and H. Krakauer, "First-principles calculations of piezoelectricity and polarization rotation in Pb(Zr<sub>0.5</sub>Ti<sub>0.5</sub>)O<sub>3</sub>," *Phys. Rev. B*, vol. 68, no. 1, p. 014112, 2003.
- [16] Hussin, N. H., Taib, M. F. M., Hassan, and O. H. Yahya, M. Z. A., "Theoretical study of PbZrTiO<sub>3</sub> and PbSnZrTiO<sub>3</sub> using a total-energy planewave-pseudopotential method," *Materials Research Express*, vol. 4, no. 7, p. 074001, 2017.
- [17] T. D. Huan, V. Sharma, G. A. Rossetti and R. Ramprasad, "Pathways towards ferroelectricity in hafnia," *Phys. Rev. B*, vol. 90, no. 6, p. 064111, 2014.

- [18] Q. Zeng, A. R. Oganov, A. O. Lyakhov, C. Xie, X. Zhang, J. Zhang, Q. Zhu, B. Wei, I. Grigorenko, L. Zhang, and L. Cheng, "Evolutionary search for new high-k dielectric materials: methodology and applications to hafnia-based oxides." *Acta Crystallographica Section C: Structural Chemistry*, vol. 70, no. 2, pp. 76-84, 2014.
- [19] Rabe, Karin M., Charles H. Ahn, and Jean-Marc Triscone, eds. *Physics of ferroelectrics: a modern perspective*. Vol. 105. Springer Science & Business Media, 2007.
- [20] A. Saeidi, F. Jazaeri, I. Stolichnov, and A. M. Ionescu, "Double-gate negative-capacitance MOSFET with PZT gate-stack on ultra thin body SOI: An experimentally calibrated simulation study of device performance," *IEEE Trans. Electron Devices*, vol. 63, no. 12, pp. 4678-4684, Dec. 2016.
- [21] Landau, L. D., and I. M. Khalatnikov. "On the anomalous absorption of sound near a second order phase transition point." *Dokl. Akad. Nauk SSSR*. Vol. 96. 1954.